Journal of Catalysis 277 (2011) 154–163

Contents lists available at ScienceDirect

Journal of Catalysis

journal homepage: www.elsevier.com/locate/jcat

Flame-made MoO_3/SiO_2–Al_2O_3 metathesis catalysts with highly dispersed and highly active molybdate species

Damien P. Debecker [a,*], Bjoern Schimmoeller [b,*], Mariana Stoyanova [c], Claude Poleunis [d], Patrick Bertrand [d], Uwe Rodemerck [c], Eric M. Gaigneaux [a]

[a] Institute of Condensed Matter and Nanoscience – Molecules, Solids and Reactivity (IMCN/MOST)[1], Université catholique de Louvain, Croix du Sud 2/17, 1348 Louvain-La-Neuve, Belgium
[b] Particle Technology Laboratory, Institute of Process Engineering, Department of Mechanical and Process Engineering, ETH Zurich, CH-8092 Zurich, Switzerland
[c] Leibniz-Institut für Katalyse e.V. an der Universität Rostock, Albert-Einstein-Str. 29a, D-18059 Rostock, Germany
[d] Institute of Condensed Matter and Nanoscience – Bio- and Soft Matter (IMCN/BSMA), Université catholique de Louvain, Croix du Sud 1, 1348 Louvain-La-Neuve, Belgium

ARTICLE INFO

Article history:
Received 7 October 2010
Revised 3 November 2010
Accepted 5 November 2010
Available online 13 December 2010

Keywords:
Flame spray pyrolysis
Propylene metathesis
Dispersion
Supported molybdenum oxide
Alkene valorisation
Si–Al mixed oxide
Carbene

ABSTRACT

MoO_3/SiO_2–Al_2O_3 catalysts are prepared via flame spray pyrolysis and evaluated in the self-metathesis of propene to ethene and butene. Their specific surface area ranges between 100 and 170 $m^2\,g^{-1}$ depending on the MoO_3 loading (1–15 wt.%, corresponding to Mo surface density between 0.3 and 6.1 Mo atoms per nm^2). The catalysts were characterized by N_2-physisorption, X-ray diffraction (XRD), Raman spectroscopy, transmission electron microscopy (TEM), X-ray photoelectron spectroscopy (XPS) and time of flight secondary ion mass spectroscopy (ToF-SIMS). The silica–alumina matrix condenses first in the flame and forms non-porous spherical particles of 5–20 nm, followed by the dispersion of Mo oxide at their surface. Depending on the MoO_3 loading, different MoO_x species are stabilized: dispersed and amorphous molybdates (mono- and oligomeric) at low loadings (<5 wt.%, <1.5 Mo nm^{-2}) and crystalline MoO_3 species at higher loadings. Raman spectroscopy suggests the presence of monomeric species for surface densities of 0.3, 0.5 and 0.8 Mo nm^{-2}. The formation of Mo—O—Mo bonds is, however, clearly established by ToF-SIMS from surface densities as low as 0.5 Mo nm^{-2}. At 1.5 Mo nm^{-2}, crystallites of β-MoO_3 (2–3 nm) are detected and further increasing the loading induces the formation of bigger α- and β-MoO_3 crystals (around 20 nm). The speciation of Mo proves to have a marked impact on the metathesis activity of the catalysts. Catalysts with high Mo loading and exhibiting MoO_3 crystals are poorly active, whereas catalysts with low Mo loading (<5 wt.%) perform well in the reaction. The catalyst loaded with only 1 wt.% of MoO_3 (0.3 Mo nm^{-2}) is the most active, reaching turn over frequencies seven times higher than reference catalysts reported in the literature. Moreover, the specific metathesis activity is clearly inversely correlated to the degree of condensation of the molybdenum oxide phase (as evaluated by ToF-SIMS). The latter finding indicates that monomeric MoO_x species are the main active centres in the olefin metathesis.

1. Introduction

Light olefin metathesis attracts particular interest for the petrochemical industry as it enables the conversion of olefins as a function of the market demand [1]. As a thermoneutral reaction it can be run at low energy and environmental cost. Catalyst recovery and ease of product separation make heterogeneous catalysis appropriate to industrial-scale production [2]. In this regard, supported molybdenum oxide systems have been widely investigated as active olefin metathesis catalysts [3]. A higher activity has been observed for SiO_2–Al_2O_3 supported MoO_3 catalyst compared to Mo oxide supported on pure SiO_2 or Al_2O_3 supports [4–6]. This higher performance has been explained by the higher acidic character of the silica–alumina surface [4].

Such silica–alumina supported MoO_3 catalysts have been synthesized via different chemistry-based methods in the liquid phase, such as impregnation [6–8], non-hydrolytic sol–gel method [9] and $MoO_2(acac)_2$ anchoring [5,8] or via dry methods such as thermal spreading [10–12]. These conventional methods allow only limited control over physical properties of the materials and, except for the non-hydrolytic sol–gel process, are all multi-step methods, thus time demanding and requiring pre-made supports. Generally, impregnated catalysts with Mo surface densities <1.0 Mo atom

* Corresponding authors. Fax: +32 10473649 (D.P. Debecker), fax: +41 44 632 12 76 (B. Schimmoeller).
E-mail addresses: damien.debecker@uclouvain.be (D.P. Debecker), schimmoeller@ptl.mavt.ethz.ch (B. Schimmoeller), eric.gaigneaux@uclouvain.be (E.M. Gaigneaux).
[1] Note: IMCN and MOST are new research entities involving the group formerly known as "Unité de catalyse et chimie des matériaux divisés".

0021-9517/$ - see front matter © 2010 Elsevier Inc. All rights reserved.
doi:10.1016/j.jcat.2010.11.003

per nm^2 exhibiting dominantly amorphous MoO_x species gave satisfactory activity [6,7,9] while crystalline MoO_3 does not show catalytic activity [13]. Accordingly, catalysts with higher Mo surface densities usually are less active and are to be avoided [7].

Therefore, a catalyst preparation method that yields Mo centres with high dispersion on the support surface is of interest. An attractive way to synthesize supported catalysts is by flame spray pyrolysis (FSP) [14–17]. This single-step process can be applied to a wide variety of precursors to produce mixed metal oxide nanoparticles with closely controlled characteristics such as stoichiometry, material morphology [18] and various other physical properties (crystallinity, thermal stability, etc.) [19] with high reproducibility and purity [20]. Furthermore, this synthesis method usually yields good dispersivities of transition metal oxide supported catalyst as shown for V_2O_5/TiO_2 [21,22] and V_2O_5/SiO_2 [23]. As Schimmoeller et al. [24] have shown in the case of Pt/Al_2O_3 catalyst, fine tuning of the acidity of the support with SiO_2 doping is also possible with this synthesis route. Catalysts containing 20–30 wt.% SiO_2 appear to be the most acidic ones [24].

Here, we report FSP synthesis of $MoO_3/SiO_2–Al_2O_3$ catalysts where the MoO_3 loading was varied from 1 wt.% up to 15 wt.%. The silica to alumina ratio is kept constant (30 wt. SiO_2–70 wt.% Al_2O_3). The catalysts were characterized by nitrogen physisorption, X-ray diffraction (XRD), X-ray photoelectron spectroscopy (XPS), transmission electron microscopy (TEM) coupled with energy dispersive X-ray spectroscopy (EDXS), Raman spectroscopy and time of flight secondary ion mass spectroscopy (ToF-SIMS). Their activity was measured in the self-metathesis of propene.

2. Experimental

2.1. Catalyst preparation

Molybdenum 2-ethylhexanoate (15% Mo, Strem Chemicals), hexamethyldisiloxane (HMDSO, Fluka, >98%), aluminium acetylacetonate (Aldrich, 99%) dissolved in a 2:1 mixture of 2-ethylhexanoic acid/acetonitrile (0.4 M) were used as molybdenum, silicon and aluminium precursors, respectively. The appropriate precursor amounts were mixed with xylene. The total support metal (Si + Al) concentration was kept constant at 0.4 M. The support composition for the catalysts based on mixed $SiO_2–Al_2O_3$ support was 30 wt.% SiO_2 and 70 wt.% Al_2O_3 [24]. The molybdenum oxide loading ranged from 1 to 15 wt.%. The $MoO_3/SiO_2–Al_2O_3$ powders were produced in a laboratory scale FSP reactor in a classical open apparatus with a precursor solution flow rate of 5 ml min^{-1} and dispersion gas (O_2, PanGas, 99.95%) flow rate of 5 l min^{-1}. The experimental setup for the synthesis of nanoscale powders by FSP is described in detail elsewhere [18,25]. The liquid precursor was fed into the reactor nozzle by a syringe pump (Inotech R232). Product particles were collected with aid of a vacuum pump (Busch SV 1025 B) on a glass microfiber filter (Whatman GF/D, 257 mm diameter) placed in a water-cooled holder. The samples are abbreviated as xMoSiAl in which x denotes the MoO_3 content in wt.% and some of their properties are given in Table 1.

2.2. Catalyst characterization

The specific surface area (SSA) of the powders was determined by a five point nitrogen adsorption isotherm at −196 °C according to the Brunauer–Emmett–Teller (BET) method (Micromeritics Tristar 3000). The sample was degassed in N_2 at 150 °C for 1 h prior to analysis. Accounting for the catalyst composition in the powder density, the average particle size (d_{BET}) was calculated assuming spherical particles.

X-ray diffraction patterns of all the powders were measured with a Bruker AXS D8 Advance device (40 kV, 40 mA) operated with monochromatized Cu Kα radiation (λ = 1.5405 Å).

Raman spectroscopy was performed with a Renishaw InVia Reflex Raman system equipped with a 785-nm laser (diode solid-state laser, 30 mW) as the excitation source focused via a microscope (Leica, magnification 50×). The spectra were recorded under dehydrated conditions with 15–25 accumulations to obtain sufficient signal-to-noise ratio and collected on a CCD camera after being diffracted by a prism. Spectra were recorded at 500 °C flushed with synthetic air as described by Schimmoeller et al. [21].

X-ray photoelectron spectroscopy (XPS) was performed on a Kratos Axis Ultra spectrometer (Kratos Analytical – Manchester – UK) equipped with a monochromatized aluminium X-ray source (powered at 10 mA and 15 kV). The pressure in the analysis chamber was about 10^{-6} Pa. The analysed area was 700 μm × 300 μm. The pass energy of the hemispherical analyser was set at 160 eV for the wide scan and 40 eV for narrow scans. Charge stabilization was achieved by using the Kratos Axis device. The electron source was operated at 1.8 A filament current and a bias of −1.1 eV. The charge balance plate was set at −2.8 V. The sample powders were deposited onto a double face tape. The following sequence of spectra was recorded: survey spectrum, C 1s, O 1s, Si 2p, Al 2p, Mo 3d and C 1s again to check for charge stability as a function of time and for the absence of degradation of the sample during the analyses. The binding energy (BE) values were referred to the C-(C, H) contribution of the C 1s peak fixed at 284.8 eV. Molar fractions (%) were calculated using peak areas normalized on the basis of acquisition parameters after a linear background subtraction, with experimental sensitivity factors and transmission factors provided by the manufacturer.

ToF-SIMS measurements were performed with an IONTOF V spectrometer. The samples were bombarded with pulsed Bi^+ ions (30 keV). The analysed area used in this work was a square of 500 × 500 μm^2, and the acquisition time was 60 s. Charge effects were compensated by means of an interlaced pulsed electron flood gun (E_k = 20 eV). With these parameters, the primary ion dose density was lower than 2×10^{11} Bi^+/cm^2. The powders were pressed with a spatula onto the adhesive side of "Post-it®" pieces.

For transmission electron microscopy (TEM), the material was dispersed in ethanol and deposited onto a perforated carbon foil

Table 1
Chemical composition, surface area, estimated particle size, and Mo surface density of FSP samples.

	Al_2O_3 (wt.%)	SiO_2 (wt.%)	MoO_3 (wt.%)	SSA ($m^2 g^{-1}$)	d_{BET} (nm)[a]	Mo surface density (at. nm^{-2})[b]
1MoSiAl	69.3	29.7	1.0	167	10.0	0.3
2MoSiAl	68.6	29.4	2.0	154	10.4	0.5
3MoSiAl	67.9	29.1	3.0	149	10.4	0.8
5MoSiAl	66.5	28.5	5.0	138	10.5	1.5
10MoSiAl	63.0	27.0	10.0	120	10.4	3.5
15MoSiAl	59.5	25.5	15.0	102	10.7	6.1

[a] Values calculated under the assumption of non-porous spherical particles.
[b] Values calculated from the nominal MoO_3 loading and under the assumption that all Mo atoms are dispersed at the surface of the particles made of silica–alumina.

supported on a copper grid. The investigations were performed on a Tecnai F30 microscope (field emission cathode, operated at 300 kV). Scanning transmission electron microscopy (STEM) images were obtained with a high-angle annular dark field (HAADF) detector.

2.3. Metathesis reaction

The evaluation of the metathesis activity of the catalysts was carried out in a multi-channel apparatus with a capacity of treating of up to 15 samples under identical conditions [26]. The whole design allows fully automated control of gas flows and of three temperature zones (gas pre-heating, reactor, and post-reactor lines with 16-port valve) along with reactor switching and product sampling. All catalysts were sieved and selected in the 200–315 μm granulometric size range. The catalysts (200 mg) were introduced in quartz straight reactors (5 mm i.d.). In each experiment, several samples were pre-treated in parallel by heating up to 550 °C (temperature ramp of 5 °C min^{-1}) in a N_2 (Air Liquide, 99.999% purity, additionally purified over molecular sieve 3 A (Roth) filter) flow of 14 ml min^{-1} in each reactor and keeping this temperature for 2 h. Afterwards, the system was cooled down to the reaction temperature (40 °C or 80 °C) under the same N_2 flow. A propene (Air Liquide, 99.95% purity, additionally purified over molecular sieve 3 A (Roth) and Oxysorb-glass (Linde) filters) flow of 8 ml min^{-1} was then admitted for about 1 h sequentially in each reactor in order to measure the initial metathesis activity of each sample. During activity measurement in a selected channel, the other reactors are kept under N_2 flow. The experiments were carried out at light overpressure (0.2 bar) in order to prevent any trace of accidental air penetration in the system.

The composition of the reaction gas was analysed by an Agilent 6890 GC. Product analysis took about 6.5 min for each injection. The separation of hydrocarbons was performed on a HP-AL/M column (30 m length, 0.53 mm i.d., 0.15 μm film thickness) applying a temperature ramp between 90 and 140 °C and FID detection.

The activity is calculated on the basis of metathesis products (ethene and *trans*- and *cis*-butene) formation. The specific activity is defined as the number of moles of propene converted to metathesis products per gram of catalyst and per hour. The standard deviation for activity measurements was less than 3% in relative. The normalized specific activity (or average turn over frequency, TOF) is defined as the number of moles of propene converted to metathesis products per mole of Mo atom and per second. It is calculated as follows (as if all Mo atoms were active in the reaction):

$$TOF(s^{-1}) = \frac{specific\ activity(mol\ g^{-1}h^{-1})}{3600(sh^{-1})} \times MM_{MoO_3}(g\ mol^{-1}) \times \frac{100\ (\%)}{wt.\%\ MoO_3}$$

where MM_{MoO_3} stands for MoO_3 molar mass.

3. Results and discussion

3.1. Nitrogen adsorption

The FSP-made Mo catalysts consist in nano-sized particles with specific surface areas (BET) ranging between 102 and 162 $m^2\ g^{-1}$ (Table 1). With increasing the MoO_3 content from 1 to 15 wt.%, the SSA is decreasing from 167 to 102 $m^2\ g^{-1}$. A similar trend of decreasing SSA has been observed for V_2O_5/TiO_2 catalysts before [15] and can be attributed to phase segregation at higher vanadia content. This is in agreement with the fact that pure FSP-made MoO_3 prepared with similar (but not identical) process conditions showed significantly lower (32 $m^2\ g^{-1}$) SSA [27]. Silica–alumina mixed oxides of similar composition but without Mo exhibited a SSA of 175 $m^2\ g^{-1}$, indicating that the presence of very low MoO_3 contents had already a slight effect on the particle formation in the flame, probably facilitating particle sintering and thereby reducing the SSA. Although the change in SSA is rather big, the influence on the average primary particles size ($d_{BET} \approx 10$ nm, Table 1) is very small due to the large difference in the solid densities. Compared, however, to classic wet-chemistry derived materials, these FSP-made MoO_3/SiO_2–Al_2O_3 catalysts have a rather low SSA. In catalysts prepared by conventional two-step methods, such as anchoring [5], thermal spreading [6,10,28] or wet impregnation [4,7], the SSA is dictated by the texture of the preformed support. This depends on the Si/Al ratio [4] and on the preparation method. Many works are based on the use of a commercial mesoporous silica–alumina powder with ca. 13 wt.% of Al_2O_3 exhibiting a SSA of about 475 $m^2\ g^{-1}$ [6,7] but supports with similar composition and much lower SSA (ca. 150 $m^2\ g^{-1}$) were also used [4]. In the case of MoO_3/SiO_2–Al_2O_3 samples prepared via non-hydrolytic sol–gel, SSAs ranging from 470 to 500 $m^2\ g^{-1}$ were obtained [9]. Nevertheless, the Mo content in the flame-made catalysts was adjusted to achieve a comparable theoretical Mo surface density as in those conventional catalyst systems. Since the boiling point of the active species MoO_3 (T_{bp} = 1155 °C) is much lower compared to that of the support material ($T_{bp} \approx 2600$ °C), it is expected that MoO_3 condensate on the surface of the preformed SiO_2–Al_2O_3 particles later in the flame, as it was shown for FSP-made V_2O_5/SiO_2 [23] and V_2O_5/TiO_2 [21,22]. Assuming that all the molybdenum oxide is found on the surface of the flame-made particles, the theoretical surface densities are calculated (Table 1).

3.2. Crystallinity

In Fig. 1, the X-ray diffraction patterns of the FSP-made catalysts are shown. All samples are characterized by a broad band from 2Θ = 20° to 35°, typical of an amorphous structure. Up to 5 wt.% MoO_3 (1.5 Mo at. nm^{-2}), the catalyst does not exhibit any diffraction peak (Fig. 1). Silica–alumina supported catalysts prepared via wet impregnation or thermal spreading exhibited MoO_3 crystals at a theoretical coverage of 0.8 Mo at. nm^{-2} [7] or 1.0 Mo at. nm^{-2} [6], respectively. In the non-hydrolytic sol–gel preparation, only traces of MoO_3 crystallites were detected at theoretical surface density of 1.8 Mo at. nm^{-2} (in that case, not all the Mo atoms are present at the surface). In the present series of FSP-made catalysts, the first distinct XRD peaks are observed for the two samples

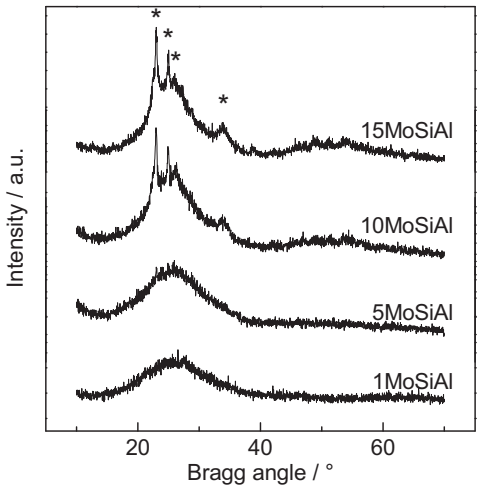

Fig. 1. X-ray diffractograms of the FSP MoO_3/SiO_2–Al_2O_3 metathesis catalysts containing 1–15 wt.% MoO_3. The '*' indicate the main diffraction lines of MoO_3 crystals (JCPDS 05-0508 and 47-1320).

containing $\geqslant$10 wt.% MoO_3 (>3.5 Mo at. nm^{-2}) at ca. 23°, 25°, 26° and 34°. These correspond to crystalline MoO_3, in the orthorhombic (α-MoO_3, main bands at 2Θ = 23.3°, 25.7°, 27.3° and 33.7°) or monoclinic (β-MoO_3, 2Θ = 23.7°, 25.9°, 27.4° and 33.7°) crystallographic phases following JCPDS 05-0508 and 47-1320, respectively. Looking at the relative intensity of the main peaks and of the reference data sheets, it appears that a mixture of both phases is probably present in the two samples.

3.3. Structure

Representative transmission electron microscopy (TEM) images are shown in Fig. 2. They reveal that the MoO_3/SiO_2–Al_2O_3 powders mainly consist in the agglomeration of aggregated spherical and non-porous particles for MoO_3 loadings up to 5 wt.%. Their size is generally in the 5–20 nm range, consistent with the average primary particle size calculated from the BET surface area (Table 1). Regular and smooth spheres are observed in the sample containing 1 wt.% MoO_3 (Fig. 2a and b). No difference in the particle morphology was visible for loadings up to 3 wt.% (not shown). In the sample containing 5 wt.% MoO_3, smaller particles (dark spots in Fig. 2c and d) are discernable at the surface of the main (support) particles. These can likely be attributed to small segregated MoO_3 particles of about 1–2 nm in size. In the samples with the highest loading (Fig. 2e and f), the particles generally appear less spherical and show more sinter necks as well as large (around 20 nm) cubic particles, which can be attributed to the presence of large MoO_3 crystals consistent with BET and XRD (Fig. 1) analyses.

3.4. Nature of the Mo species

Raman spectroscopy was used to investigate the nature of the Mo species stabilized at the surface of the catalysts (Fig. 3). The measurements have been performed in dehydrated conditions (500 °C in synthetic air). At low loading (1–3 wt.% of MoO_3), the typical spectra of isolated MoO_x supported species are obtained. No band related to Mo—O—Mo bonds is detected (signals expected in the 850–870 cm^{-1} range). The signal at ca. 1001 cm^{-1} corresponds to the Mo=O stretching and the broad band at 310–370 cm^{-1} is due to the Mo=O bending mode [29]. It can be noted that the peak at ca. 1001 cm^{-1} is somewhat asymmetric. This indicates the presence of isolated monomolybdates in distorted tetrahedral coordination with two terminal Mo=O and two bridging Mo—O-support bonds, even if the presence of species in a monooxo configuration with four anchoring Mo—O-support bonds cannot be ruled out [30].

Additional signals are observed on the samples with higher loadings. For the 5MoSiAl catalyst (1.5 Mo at. nm^{-2}), two weak bands are detected at 849 cm^{-1} and 774 cm^{-1}, which can be attributed to the crystalline β-MoO_3 phase [31,32]. These were not detected by XRD (Fig. 1) due to the small size of the particles (1–2 nm by TEM, Fig. 2d), below the detection limit of X-ray diffraction (ca. 3 nm). It should be noted that for catalysts prepared by conventional impregnation methods Raman analysis showed MoO_3 crystallites at a Mo surface density of 0.8 Mo at. nm^{-2} on silica and from 5.0 Mo at. nm^{-2} on alumina [33]. On a silica-rich silica–alumina support, MoO_3 crystals were detected by Raman at 0.8 Mo at. nm^{-2} as well [7], still significantly lower than for FSP-made materials presented here. At higher loading, these bands get more intense and an additional band at 820 cm^{-1} is detected in the 10MoSiAl and 15MoSiAl catalysts. The latter corresponds to the crystalline α-MoO_3 phase [32].

Noticing the evolution of the intensity of the signals related to the α and β phases in the catalysts with high loading, it appears that a progressive phase change occurs from the less stable β-MoO_3 phase formed in the catalysts with intermediate loading to the more stable α-MoO_3 phase formed in the catalysts with the highest loading. Considering the results of XRD (Fig. 1) and TEM analysis (Fig. 2), the phase transition of β to α seems also to be size dependent with the β phase being favoured at small crystallite sizes while with increasing MoO_3 crystal size more and more α phase is formed.

As far as the Mo=O stretching band is concerned, a progressive shift from ca. 1001 cm^{-1} to ca. 993 cm^{-1} is observed upon MoO_3 loading increase in the 1–15 wt.% range. In addition, the asymmetry of the peak appears more pronounced and weak shoulders are distinguished. Various MoO_x species thus appear to coexist in these samples (monomeric, polymeric, and crystalline Mo oxide). It is, however, delicate to enter into interpretations of the slight changes in the energy of this band since it is known that the Mo=O modes within monomeric and polymeric Mo surface species usually overlap [30,33,34]. In addition, the Mo=O stretching mode in MoO_3 crystals is also expected at 996 cm^{-1} [34].

3.5. Surface characterization

In order to further clarify the structure of the present MoO_x species, the composition of the sample surfaces has been analysed by XPS. Table 2 provides the molar fraction of each detected element. When the loading increases from 1 to 15 wt.%, the Mo surface concentration proves to increase linearly and the Al and Si surface concentrations decrease. This is qualitatively in agreement with the stated particle formation mechanism in which the support forms first in the flame and subsequently MoO_x condensates on the surface. The Mo 3d peak is characterized by a well-defined doublet directly attributable to Mo^{VI}. Its binding energy (BE) tends to shift to higher energy – closer to the case of pure molybdenum trioxide (233.1 eV) – when the loading increases. The low BE (ca. 332.8 eV) measured for the catalyst with low loading (5 wt.% and lower) indicates that MoO_x species interact strongly with the silica–alumina matrix. The high BE (>333.0 eV) found in 10MoSiAl and 15MoSiAl shows that a pure MoO_3 phase with limited interaction with the support is formed at the surface of these samples corroborating the results of the previous analysis. The peak width decreases regularly as the MoO_3 loading increases. This confirms the transition from dispersed and interacting surface MoO_x species to a well-defined MoO_3 phase [9].

Looking at the surface Mo/(Si + Al) atomic ratio provides information about the location of Mo atoms with respect to the silica–alumina matrix. Fig. 4 was drawn to show the evolution of the surface Mo/(Si + Al) atomic ratio as a function of the nominal bulk Mo/(Si + Al) atomic ratio (calculated from the nominal composition of each sample, Table 1). This ratio increases linearly with the loading. Obviously, the surface ratio is markedly higher than the nominal bulk ratio (dotted line, Fig. 4), which shows unambiguously that the surface is rich in Mo. In other words, Mo atoms tend to cover the silica–alumina matrix, which again quantitatively corroborates the proposed particle formation route stated earlier.

Further insights into the chemistry of the catalysts surface are obtained via time of flight secondary ion mass spectroscopy (ToF-SIMS). The technique is based on the analysis of the secondary ions that are ejected from the surface under irradiation with a flux of (30 keV) Bi^+ cations. The method is particularly powerful to probe the composition of the outermost surface of solid samples and to understand the way surface atoms interact with each others, which is of great importance in the field of heterogeneous catalysis [9,35,36]. In the negative spectra, the following ions have been observed and quantified: C^-, CH^-, O^-, OH^-, F^-, C_2H^-, Al^-, Si^-, O_2^-, Cl^-, AlO^-, AlO_2^-, SiO_2^-, SiO_3^-, MoO^-, MoO_2^-, MoO_3^-, MoO_4^-, $Mo_2O_6^-$, $Mo_2O_7^-$, $Mo_2O_8Al^-$, $Mo_3O_9^-$, $Mo_3O_{11}Al^-$, $Mo_4O_{12}^-$, $Mo_4O_{14}Al^-$, $Mo_5O_{16}^-$, $Mo_5O_{17}Al^-$. For one given sample, the relative intensity of each fragment is calculated by dividing its intensity by the

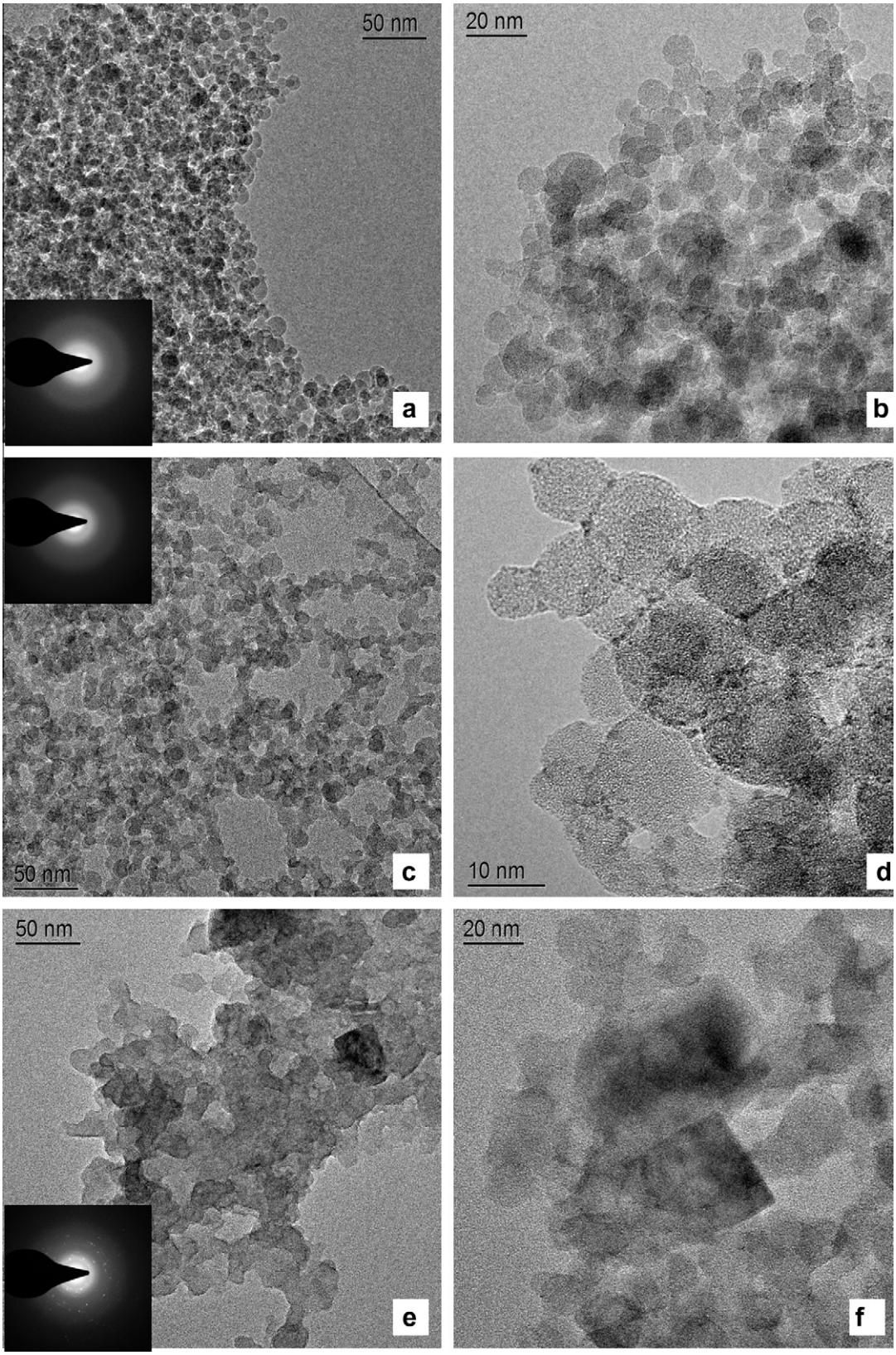

Fig. 2. Typical TEM micrographs of 1MoSiAl (a and b), 5MoSiAl (c and d) and 15MoSiAl (e and f). Insets are the EDX patterns. Note: 2MoSiAl and 3MoSiAl looked like 1MoSiAl; 10MoSiAl looked like 15MoSiAl.

sum of the contributions of all above-mentioned anions (total counts). The relative intensities of given fragments can then be compared from one sample to another. A complete quantification table is available as Supplementary material.

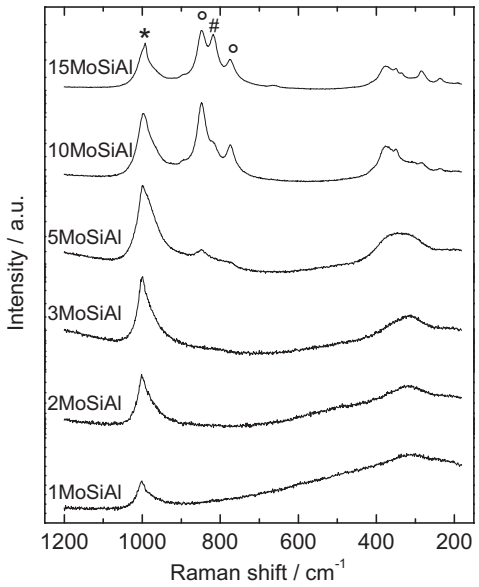

Fig. 3. Raman spectra of the FSP MoO_3/SiO_2–Al_2O_3 metathesis catalysts. Spectra were recorded under dehydrated conditions at 500 °C. Symbols indicate nature of the main bands: Mo=O terminal stretching mode in different species (*); Mo—O—Mo stretching mode in α-MoO_3 (#) and in β-MoO_3 (○).

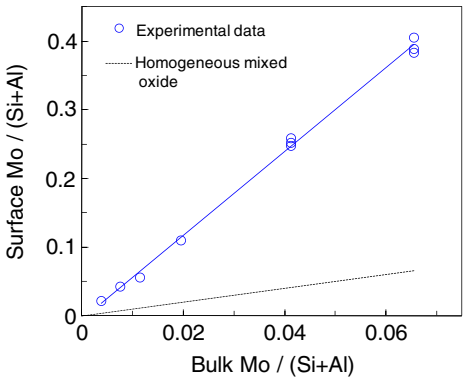

Fig. 4. Atomic Mo/(Si + Al) ratio measured at the surface of the xMoSiAl catalysts via XPS as a function of the nominal bulk atomic Mo/(Si + Al) ratio. For some samples, the measurements have been repeated three times, showing excellent reproducibility. The dotted line represents the situation expected for homogeneous mixed oxides (namely, equal surface and bulk Mo/(Si + Al) ratio). The plain line is a linear interpolation between experimental data point.

The main Mo-containing fragments have been particularly studied and are shown in Fig. 5. On the catalyst with the lowest loading (1MoSiAl), the presence of Mo is readily witnessed by the detection of MoO_x^- fragments (partial ToF-SIMS spectra presented in Fig. 5a). Visibly, the relative intensity of the fragments containing one Mo atom (such fragments containing only one Mo atom are denoted "mono-Mo" clusters below) increases when the loading increases from 1 to 5 wt.% MoO_3. Upon further increase in the loading, the contribution of these mono-Mo fragments does not seem to increase noticeably. Fig. 5b and c show the evolution of the fragments containing, respectively, two or three Mo atoms. These clusters, along with all other clusters containing more than one Mo atom, are referred to as "poly-Mo" clusters. The detection of such clusters implies the occurrence of Mo—O—Mo bridges. It is an evidence for the presence, at the outermost surface of the solids, of agglomerated forms of Mo oxide (oligomers, polymers or crystals) [9]. These fragments prove to increase in intensity upon loading increase. Qualitatively, it can be noticed that poly-Mo clusters are virtually absent in the 1MoSiAl sample (only traces of $Mo_2O_6^-$ may barely be distinguished in the noise of the spectra). This observation, conjugated to the detection of mono-Mo fragments suggests the presence of isolated MoO_x species in this sample. In all other catalysts, $Mo_2O_6^-$, $Mo_2O_7^-$, $Mo_2O_8Al^-$, $Mo_3O_9^-$ and $Mo_3O_{11}Al^-$ clusters are always detected. Poly-Mo clusters with higher mass are also detected, especially on the samples with high loading (>5 wt.%). Thus, while Raman spectroscopy failed to detect the presence of oligo- or polymeric MoO_x species in catalysts with relatively low loading (because the Mo=O stretching band overlaps with the band of monomeric species and because the response for the Mo—O—Mo stretching mode is too low), ToF-SIMS evidences the presence of such species by highlighting the occurrence of oxo bridges between Mo atoms. Oligo- or polymeric molybdates are significantly detected at the surface of the catalysts with loading $\geqslant$2 wt.% (0.5 Mo nm^{-1}).

For the catalysts with loadings >5 wt.%, it appeared already clearly from XRD, Raman and TEM experiments that polymeric MoO_x species or even MoO_3 crystallites are formed at the support surface. ToF-SIMS data offer the possibility to discuss quantitatively the degree of condensation (or agglomeration) of the MoO_x species. For that purpose, the "poly-Mo/(poly-Mo + mono-Mo)" ratio has been calculated. In this ratio, the term "poly-Mo" refers to the sum of the relative intensity of all clusters containing more than one Mo atom, and the term "mono-Mo" refers to the sum of all clusters containing only one Mo atom. This ratio is expected to be very low in the case of highly dispersed species (low degree of condensation and low amount of Mo—O—Mo bridges) and high for highly agglomerated species like polymolybdates or crystals. Pure MoO_3 (Aldrich 99.5%), consisting of large MoO_3 crystals, has been analysed by ToF-SIMS as a reference in the same experimental conditions, resulting in a "poly-Mo/(poly-Mo + mono-Mo)" ratio equal to 0.76. In the same way, pure MoO_3 was prepared by FSP and analysed in ToF-SIMS. These powders made of high surface area MoO_3 nanoparticles yielded a "poly-Mo/(poly-Mo + mono-Mo)" ratio of 0.63, significantly lower than for the commercial sample, which may be attributed to the higher SSA of the flame-made sample. These values can be taken as a reference for the cases where the degree of condensation is maximal for micron- (0.76) or nano-sized (0.63) molybdenum oxide. The same ratio reaches only 0.26 and 0.28 for 10MoSiAl and 15MoSiAl, respectively. This shows that even if crystalline MoO_3 is formed at the surface of these catalysts, other MoO_x species which are less

Table 2
Surface composition determined via XPS, position and width of the Mo $3d_{3/2}$ peak.

	Mo (at.%)	Si (at.%)	Al (at.%)	O (at.%)	C (at.%)	Mo $3d_{3/2}$ BE (eV)	Mo $3d_{3/2}$ fwhm (eV)
1MoSiAl	0.65	9.27	20.61	55.36	14.11	332.8	2.6
2MoSiAl	1.23	8.49	20.50	54.10	15.68	332.7	2.4
3MoSiAl	1.59	7.97	20.41	52.96	17.08	332.8	2.3
5MoSiAl	2.74	7.51	17.38	54.26	18.12	332.9	2.1
10MoSiAl	5.48	6.77	14.91	54.83	18.01	333.2	1.7
15MoSiAl	7.46	5.70	13.32	53.19	20.33	333.1	1.6

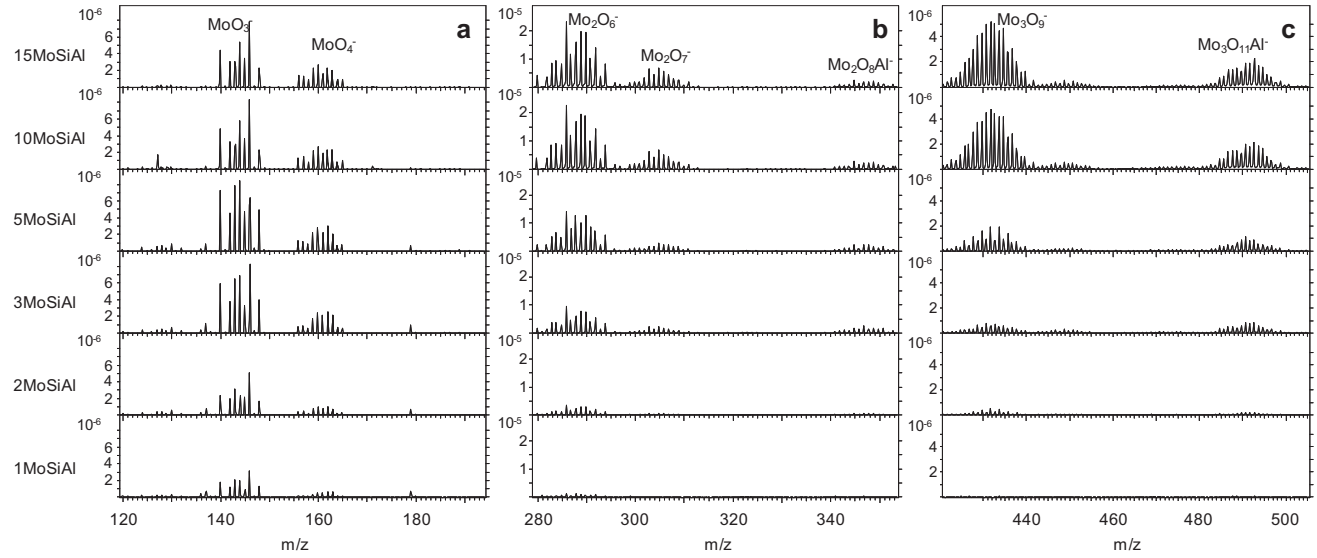

Fig. 5. Partial negative ToF-SIMS spectra of the FSP catalysts (relative intensity). *Y*-axis scale of each part of spectra is kept constant for all catalysts. The samples are labelled on the left of the figure. (a) In the 120–195 *m/z* range, the MoO_3^- and MoO_4^- fragments are followed at ca. 145 and 162, respectively. (b) In the 280–355 *m/z* range, the $Mo_2O_6^-$, $Mo_2O_7Al^-$ and $Mo_2O_8Al^-$ fragments are followed at ca. 288, 305 and 348, respectively. (c) In the 420–505 *m/z* range, the $Mo_3O_9^-$ and $Mo_3O_{11}Al^-$ are followed at ca. 432 and 493, respectively.

agglomerated than bulky MoO_3 crystals are also present (e.g. 2-D oligo- or polymolybdates, monomeric species).

As far as the catalysts with low loading (<5 wt.%) are concerned, Raman characterization suggests the presence of highly dispersed species, namely monomeric and oligo- or polymeric MoO_x species. The deposition of such amorphous and dispersed phase may occur either (i) in a *cooperative* way, namely with several Mo atoms getting condensed together at the surface of the particles and forming "patches" of oligo- or polymolybdates or (ii) in an *independent* way, namely with monomeric species being deposited randomly at the surface of the support. In the first case, Mo—O—Mo bridges would readily exist, even at very low MoO_3 loading. Moreover, the proportion of mono-Mo clusters and poly-Mo clusters detected in ToF-SIMS would remain rather constant. In the second case, the occurrence of truly monomeric species would be possible at low loading and the proportion of Mo—O—Mo bridges should increase statistically with the increase in MoO_3 loading (as the available surface is limited, Mo atoms would progressively have a higher probability to have other Mo atoms as direct neighbours). Fig. 6 (left axis) is an argument in favour of the second hypothesis. The proportion of poly-Mo increases clearly when the loading increases. Overall, ToF-SIMS results allow describing in further detail the four samples with the lowest loading: (i) the 1MoSiAl sample exhibits dominantly monomeric MoO_x species, (ii) upon increase in the loading, the proportion of oligo- or polymeric molybdates increases noticeably and (iii) initial formation and dispersion of the isolated MoO_x species happens randomly on the support surface without any indication of preferential localized deposition.

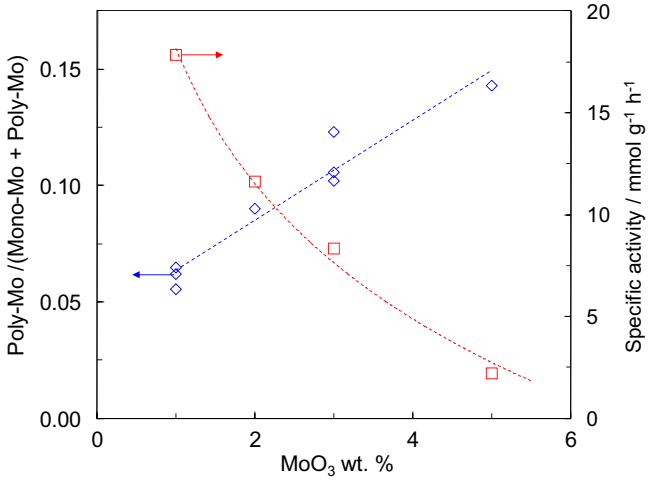

Fig. 6. Proportion of poly-Mo clusters detected in ToF-SIMS for the xMoSiAl catalysts containing 1–5 wt.% MoO_3 (◇; left *Y*-axis) and specific activity of the same catalysts in the self-metathesis of propene at 40 °C (□; right *Y*-axis). The ToF-SIMS measurement and the evaluation of the poly-Mo/(mono-Mo + poly-Mo) ratio have been repeated three times on 1MoSiAl and 3MoSiAl, showing good reproducibility. The term "Mono-Mo" refers to the sum of the relative intensities of all clusters containing one Mo atom. The term "Mono-Mo" refers to the sum of the relative intensities of all clusters containing more than one Mo atom. The standard deviation for metathesis measurement was checked to be smaller than 3% in relative.

3.6. Metathesis activity

The activity of all samples has been measured in the self-metathesis of propene at 40 °C and 80 °C, after activation in N_2 at 550 °C. In Fig. 7, the activity as a function of time is presented for catalysts with 1–5 wt.% MoO_3 loading. 10MoSiAl and 15MoSiAl were found to be poorly active (vide infra, Table 3). From these tests, it appears that the MoO_3 loading has a marked influence on the metathesis activity. At 40 °C, the activity increases first before reaching steady-state conditions after approximately 30 min of reaction time. The activity decreases when the loading increases. Changing the reaction temperature does not modify the ranking of the catalysts in terms of performances. The reaction temperature, however, influences the activity as well as the stability of the catalysts. At 80 °C, higher initial activity can be reached but it results at the same time in a faster deactivation rate not reaching steady-state conditions, even after one hour of reaction time (Fig. 7).

Catalytic performance (activity, selectivity) was compared at steady-state conditions (i.e. 46 min of reaction) for the different catalysts (Table 3). At 40 °C, the selectivity to primary metathesis products is excellent, typically above 99%. Traces of secondary

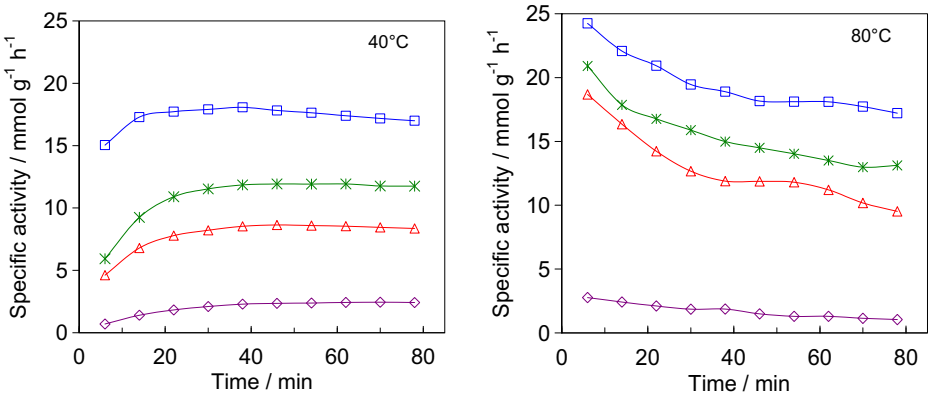

Fig. 7. Specific activity of (□) 1MoSiAl, (*) 2MoSiAl, (Δ) 3MoSiAl and (♦) 5MoSiAl as a function of time and measured at (left) 40 °C and (right) 80 °C.

Table 3
Specific metathesis activity and selectivity of FSP catalysts (at 46 min time-on-stream).

40 °C			80 °C	
Catalyst	Specific activity[a]/mmol g^{-1} h^{-1} (TOF/$mmol_{propene}$ mol_{Mo}^{-1} s^{-1})	Selectivity[b] (%)	Specific activity[a]/mol g^{-1} h^{-1} (TOF/$mmol_{propene}$ mol_{Mo}^{-1} s^{-1})	Selectivity[b] (%)
1MoSiAl	17.8 (71.3)	99.7	18.2 (72.8)	98.5
2MoSiAl	11.9 (23.9)	99.2	14.5 (29.0)	98.6
3MoSiAl	8.6 (11.4)	99.6	11.9 (15.9)	98.4
5MoSiAl	2.3 (1.9)	99.4	1.5 (1.2)	96.4
10MoSiAl	1.5 (0.6)	99.4	0.9 (0.4)	96.2
15MoSiAl	1.4 (0.3)	99.5	0.5 (0.1)	94.7

[a] Activity calculated on the basis of the product formation (ethene, *cis*- and *trans*-butene).
[b] Selectivity to primary metathesis products. The balance is obtained with products of isomerisation and secondary metathesis products.

metathesis products (pentenes and hexenes) and of isomerisation products (1-butene, isobutene) complete the carbon balance. The selectivity to direct metathesis products at 80 °C remains very high (>98% for <5 wt.% MoO_3) but is slightly lower than at 40 °C. Clearly, the increase in reaction temperature enhances the rate of the sought for metathesis reaction but also of the side reactions (secondary metathesis and isomerisation). Low reaction temperature appears more relevant if very high selectivity is pursued. In addition, it is well known that the active carbene centres are fragile and prone to deactivation under higher reaction temperature [3], which is confirmed here.

The specific activity decreases dramatically upon increase in the MoO_3 loading (Table 3). The specific activity ranges from 1.4 mmol g^{-1} h^{-1} for the least active 15MoSiAl to 17.8 mmol g^{-1} h^{-1} for the most active 1MoSiAl. As a point of comparison, similar metathesis catalysts prepared via classical impregnation of ammonium heptamolybdate (AHM) on a silica–alumina support or by thermal spreading and with MoO_3 loading in the 8–17 wt.% range (0.8–1.7 Mo at. nm^2) reached classically 12–16 mmol g^{-1} h^{-1} under the same experimental conditions [4,7,10]. Thus, in the present study, only 1MoSiAl and 2MoSiAl – with much lower Mo loading and Mo surface density (0.3 and 0.5 Mo at. nm^2 respectively) – prove to be good metathesis catalysts, with specific activity in the same range or slightly higher.

It must be recalled that previous kinetic studies have demonstrated that only a small proportion of Mo atoms present in MoO_3-based heterogeneous metathesis catalysts (~1%) turns out to be active [37]. In this context, the activity is often conveniently expressed as an average activity per atom of molybdenum present in the catalyst. This value is sometimes called a turn over frequency (TOF). It must be kept in mind that it is an average value for all Mo atoms and not the actual activity of each working centre. It is expressed in moles of propene converted to metathesis products per mole of Mo atoms and per unit of time. While the specific activity indicates a decrease of only 44% (1MoSiAl vs. 2MoSiAl, Table 3) when increasing the MoO_3 loading from 1 to 2 wt.%, the effect is much more pronounced when looking at the TOF. Latter decreases by 77% (from 71.3 to 23.9 $mmol_{propene}$ mol_{Mo}^{-1} s^{-1}) when doubling the MoO_3 content. The best catalysts based on supported MoO_x studied by Handzlik et al. in very similar activation and reaction conditions and with similar catalysts obtained via impregnation of AHM, anchoring or thermal spreading of bis(acetyloacetonato)-dioxomolybdenum reached TOFs of about 10 $mmol_{propene}$ mol_{Mo}^{-1} s^{-1} [5,6], seven times smaller than the values measured for the most active flame-made catalysts (1MoSiAl, Table 3). Balcar et al. working with similar catalysts for the metathesis of higher 1-alkenes reported 8 $mmol_{propene}$ mol_{Mo}^{-1} s^{-1} [38]. In our previous studies, the observed TOFs levelled off at similar values [4,7,9,10]. This shows that a large proportion of Mo atoms present in 1MoSiAl turns out to be active. In other words, the nature of the MoO_x species (dominantly monomeric) stabilized on this catalyst is the most appropriate to generate active metathesis centres.

It should be noted that immobilized Mo–organometallic complexes grafted on pure silica can result in well-defined catalysts with higher TOF values than reported here [39,40]. In those systems, however, the active carbene centre surrounded by protecting and activating ligands is designed via multi-step organometallic chemistry and grafted on a solid carrier to yield highly active heterogeneous catalysts. Obviously, the preparation method and its price make these catalysts attractive mainly for the production of chemicals with high added value. While here we discuss MoO_3-based catalysts made by a dry one-step process, which can be considered as cheap and robust heterogeneous catalysts, mainly of interest for the conversion of huge tonnage of low cost light olefins.

Trying to interpret the activity of FSP catalysts in conjunction with their physico-chemical characterization data, the samples can be divided in two groups. On the one hand, 10MoSiAl and 15MoSiAl catalysts prove to be virtually inactive (especially in terms of TOF). This correlates with the formation of inactive crystalline MoO_3, as demonstrated by XRD, Raman and TEM. Many reports from the literature assert that crystalline MoO_3 is not active in the metathesis reaction [13]. Nevertheless, aside from these agglomerated MoO_x species more dispersed species are present (as suggested by ToF-SIMS) and yield in few active centres responsible for the low activity observed for the 10MoSiAl and 15MoSiAl samples.

On the other hand, the catalysts with lower MoO_3 loadings are significantly more active. These samples exhibited relatively different catalytic performances but proved to be very similar to each other in terms of characterization. They are totally XRD-amorphous and seem to exhibit mainly well-dispersed MoO_x species (Raman, TEM) except the 5MoSiAl catalyst. Latter, however, lies between these two groups, as small MoO_3 nanoparticles are detected in TEM (Fig. 2d) and Raman bands attributed to crystalline MoO_3 are detected (Fig. 3). For the catalysts with 1–3 wt.% of MoO_3, the differences in terms of activity cannot readily be put in parallel with differences in terms of "classical" physico-chemical properties (texture, crystallinity, structure, etc.). The only clear difference that was observed in this series of catalysts is the progressive increase in the proportion of poly-Mo clusters detected by ToF-SIMS. This ratio appears obviously linked to the catalytic activity of theses samples: when the proportion of poly-Mo clusters detected increases, the metathesis activity decreases accordingly (Fig. 6). Therefore, it appears that the best MoO_x species, yielding active metathesis centres – like in the case of 1MoSiAl – are supported truly isolated monomeric molybdates.

4. Conclusion

In this study, the possibility to prepare MoO_3/SiO_2–Al_2O_3 metathesis catalysts via the flame spray pyrolysis method was explored. Such flame-made catalysts are composed of non-porous spherical particles of silica–alumina, with a Mo oxide phase deposited on their surface. The nature of the MoO_x species stabilized at the surface is highly dependent on the nominal MoO_3 loading. Highly dispersed (monomeric) species are preferentially produced at low MoO_3 loading (1–3 wt.% of MoO_3). Bulk MoO_3 crystals are formed when the loading increases to 10–15 wt.%. At intermediate loading, segregated MoO_3 nanoparticles are observed.

Flame-made MoO_3/SiO_2–Al_2O_3 samples containing 1–3 wt.% MoO_3 were active in the self-metathesis of propene, reaching TOF of up to 73 $mmol_{propene}\ mol_{Mo}^{-1}\ s^{-1}$ (1 wt.% MoO_3, 0.3 Mo at. nm^{-2}), seven times higher as the highest turn over frequency reported for comparable MoO_3-based metathesis catalysts so far. The reaction temperature has an impact on the initial metathesis activity and on the catalyst stability. At 40 °C, the activity appears relatively stable and the selectivity to primary metathesis is close to 100%.

Only the samples with low MoO_3 loading, i.e. low Mo surface density (<0.8 Mo at. nm^{-2}), exhibit high metathesis performances. The very low activity of the catalysts with 10 or 15 wt.% of MoO_3 was ascribed to the formation of MoO_3 crystals. At low loading, the metathesis activity appears to be directly linked to the quality of the Mo oxide dispersion. ToF-SIMS experiments highlight the fact that Mo—O—Mo bridges are getting progressively infrequent when the nominal loading decreases and this can be put in parallel with the increase in the metathesis activity. In other words, this study indicates the superior activity of highly dispersed, ideally monomeric, supported molybdate species achieved by application of flame spray pyrolysis as synthesis route.

Acknowledgments

The authors thank Frank Krumeich and EMEZ (ETH Zürich) for the TEM analysis and Lisa Joss for the help with the catalyst synthesis. The authors acknowledge the Communauté française de Belgique and the Fonds National de la Recherche Scientifique (FNRS) of Belgium for their support in the acquisition of the ToF-SIMS equipment. D.P. Debecker thanks the FNRS for his Research Fellow position. The authors from IMCN/MOST are involved in the "Inanomat" IUAP network sustained by the Service public fédéral de programmation politique scientifique (Belgium), in the Cost Action D41 sustained by the European Science Foundation, in an ARC program sustained by the Communauté française de Belgique and in the European Multifunctional Material Institute (EMMI) built on the basis of the former "FAME" Network of Excellence of the EU 6th FP.

Appendix A. Supplementary material

Supplementary data associated with this article can be found, in the online version, at doi:10.1016/j.jcat.2010.11.003.

References

[1] J.C. Mol, J. Mol. Catal. A 213 (2004) 39–45.
[2] H.J. Liu, L. Zhang, X.J. Li, S.J. Huang, S.L. Liu, W.J. Xin, S.J. Xie, L.Y. Xu, J. Nat. Gas Chem. 18 (2009) 331–336.
[3] K.J. Ivin, J.C. Mol, Olefin Metathesis, Metathesis Polymerization, ed. A. Press, London, 1997.
[4] D.P. Debecker, D. Hauwaert, M. Stoyanova, A. Barkschat, U. Rodemerck, E.M. Gaigneaux, Appl. Catal. A, in press. doi:10.1016/j.apcata.2010.06.021.
[5] J. Handzlik, J. Ogonowski, J. Stoch, M. Mikolajczyk, Catal. Lett. 101 (2005) 65–69.
[6] J. Handzlik, J. Ogonowski, J. Stoch, M. Mikolajczyk, P. Michorczyk, Appl. Catal. A 312 (2006) 213–219.
[7] D.P. Debecker, M. Stoyanova, U. Rodemerck, A. Leonard, B.-L. Su, E.M. Gaigneaux, Catal. Today, in press. doi:10.1016/j.cattod.2010.07.026.
[8] J. Handzlik, J. Ogonowski, J. Stoch, M. Mikolajczyk, Appl. Catal. A 273 (2004) 99–104.
[9] D.P. Debecker, K. Bouchmella, C. Poleunis, P. Eloy, P. Bertrand, E.M. Gaigneaux, P.H. Mutin, Chem. Mater. 21 (2009) 2817–2824.
[10] D.P. Debecker, M. Stoyanova, U. Rodemerck, E.M. Gaigneaux, Stud. Surf. Sci. Catal. 175 (2010) 581–585.
[11] P. Topka, H. Balcar, J. Rathousky, N. Zilkova, F. Verpoort, J. Cejka, Microporous Mesoporous Mater. 96 (2006) 44–54.
[12] D.P. Debecker, M. Stoyanova, U. Rodemerck, P. Eloy, A. Léonard, B.-L. Su, E.M. Gaigneaux, J. Phys. Chem. C 114 (2010) 18664–18673.
[13] B. Zhang, N. Liu, Q. Lin, D. Jin, J. Mol. Catal. 65 (1991) 15–28.
[14] S. Roy, N. van Vegten, A. Baiker, J. Catal. 271 (2010) 125–131.
[15] G.L. Chiarello, M.H. Aguirre, E. Selli, J. Catal. 273 (2010) 182–190.
[16] R.D. Zhang, W.Y. Teoh, R. Amal, B.H. Chen, S. Kaliaguine, J. Catal. 272 (2010) 210–219.
[17] O. Mekasuwandumrong, S. Phothakwanpracha, B. Jongsomjit, A. Shotipruk, J. Panpranot, Catal. Lett. 136 (2010) 164–170.
[18] R. Strobel, S.E. Pratsinis, J. Mater. Chem. 17 (2007) 4743–4756.
[19] R. Strobel, A. Baiker, S.E. Pratsinis, Adv. Powder Technol. 17 (2006) 457–480.
[20] W.J. Stark, R. Strobel, D. Gunther, S.E. Pratsinis, A. Baiker, J. Mater. Chem. 12 (2002) 3620–3625.
[21] B. Schimmoeller, H. Schulz, A. Ritter, A. Reitzmann, B. Kraushaar-Czametzki, A. Baiker, S.E. Pratsinis, J. Catal. 256 (2008) 74–83.
[22] B. Schimmoeller, R. Delaigle, D.P. Debecker, E.M. Gaigneaux, Catal. Today 157 (2010) 198–203.
[23] B. Schimmoeller, Y. Jiang, S.E. Pratsinis, A. Baiker, J. Catal. 274 (2010) 64–75.
[24] B. Schimmoeller, F. Hoxha, T. Mallat, F. Krumeich, S.E. Pratsinis, A. Baiker, Appl. Catal. A 374 (2010) 48–57.
[25] L. Madler, H.K. Kammler, R. Mueller, S.E. Pratsinis, J. Aerosol Sci. 33 (2002) 369–389.
[26] U. Rodemerck, P. Ignaszewski, M. Lucas, P. Claus, Chem. Eng. Technol. 23 (2000) 413–416.
[27] J.A. Azurdia, A. McCrum, R.M. Laine, J. Mater. Chem. 18 (2008) 3249–3258.
[28] H. Balcar, P. Topka, N. Zilkova, J. Perez-Pariente, J. Cejka, Stud. Surf. Sci. Catal. 156 (2005) 795–802.
[29] A. Christodoulakis, S. Boghosian, J. Catal. 260 (2008) 178–187.
[30] A. Christodoulakis, E. Heracleous, A.A. Lemonidou, S. Boghosian, J. Catal. 242 (2006) 16–25.

[31] E.M. McCarron III, J. Chem. Soc., Chem. Commun. (1986) 336–338.
[32] T.M. Huong, K. Fukushima, H. Ohkita, T. Mizushima, N. Kakuta, Catal. Commun. 7 (2006) 127–131.
[33] H.C. Hu, I.E. Wachs, S.R. Bare, J. Phys. Chem. 99 (1995) 10897–10910.
[34] G. Mestl, T.K.K. Srinivasan, Catal. Rev. – Sci. Eng. 40 (1998) 451–570.
[35] D.P. Debecker, K. Bouchmella, R. Delaigle, P. Eloy, C. Poleunis, P. Bertrand, E.M. Gaigneaux, P.H. Mutin, Appl. Catal. B 94 (2010) 38–45.
[36] J. Grams, Eur. J. Mass Spectrom. 16 (2010) 453–461.
[37] J. Handzlik, J. Ogonowski, Catal. Lett. 88 (2003) 119–122.
[38] H. Balcar, D. Mishra, E. Marceau, X. Carrier, N. Zilková, Z. Bastl, Appl. Catal. A 359 (2009) 129–135.
[39] F. Blanc, J. Thivolle-Cazat, J.M. Basset, C. Coperet, A.S. Hock, Z.J. Tonzetich, R.R. Schrock, J. Am. Chem. Soc. 129 (2007) 1044–1045.
[40] N. Rendon, R. Berthoud, F. Blanc, D. Gajan, T. Maishal, J.M. Basset, C. Coperet, A. Lesage, L. Emsley, S.C. Marinescu, R. Singh, R.R. Schrock, Chem. Eur. J. 15 (2009) 5083–5089.